Highlights

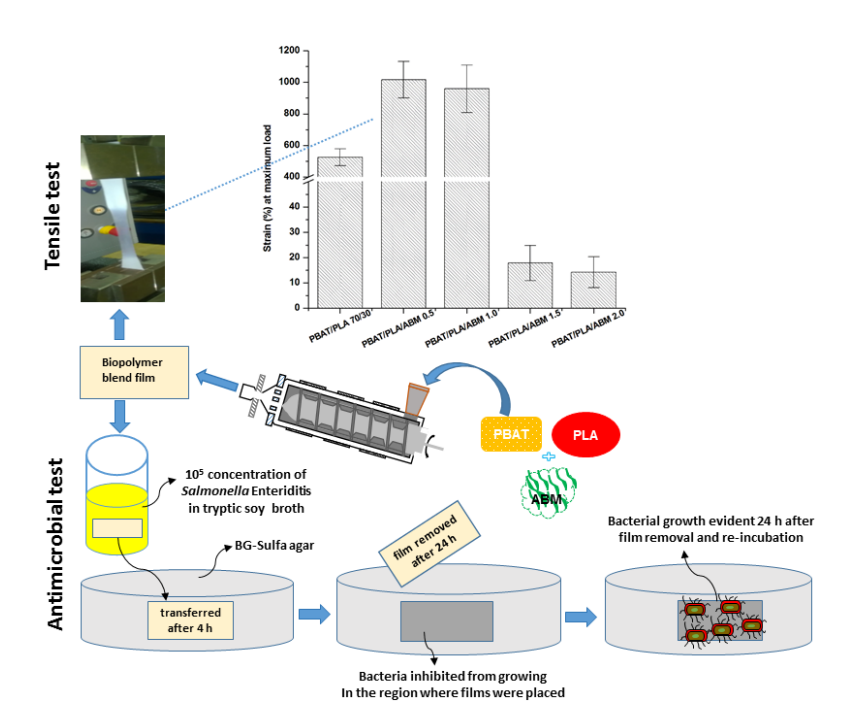
• PBAT/PLA/egg white biodegradable flexible films produced through extrusion

 Egg white has an effect on microstructure, mechanical and antimicrobial properties of PBAT/PLA blend

 Egg white significantly increased the thermal stability and toughness of PBAT/PLA blend

• The inclusion of egg white in PBAT/PLA film show significant bacteriostatic effect when in contact with bacteria

Table of Content Graphic



- 18 Tough aliphatic-aromatic copolyester and chicken egg white flexible biopolymer blend with
- 19 **bacteriostatic effects**
- 20 Boniface J. Tiimob^a, Vijaya K. Rangari^{a,*}, Gregory Mwinyelle^b, Woubit Abdela^b, Paul G. Evans^c,
- 21 Nicholas Abbott^c, Temesgen Samuel^b, Shaik Jeelani^a
- ^aDepartment of Materials Science and Engineering, ^bDepartment of Pathobiology, College of
- 23 Veterinary Medicine, Tuskegee University, Tuskegee, AL 36088, United States
- ^cDepartment of Chemical and Biological Engineering, University of Wisconsin-Madison,
- 25 Madison, WI 53706, United States
- **KEYWORDS**: bacteriostatic films, biopolymer blends, immiscible polymers, melt-extrusion
- 27 **ABSTRACT**
- 28 Extruded 70/30 poly (butylene adipate-co-terephthalate) (PBAT)/ polylactic acid (PLA) blends
- incorporated with 0.5, 1.0, 1.5 and 2 wt. % of egg white [albumen (ABM)] were investigated to
- 30 determine the effect of ABM on the microstructure and antimicrobial properties of PBAT/PLA
- 31 blend. Microstructural analysis revealed immiscibility in the two polymers, due to the presence of
- 32 distinct melting points, heterogeneous phase and vibrational frequencies unique to each polymer.
- 33 Thermal and tensile testing also suggests that the inclusion of ABM tailored the blend and
- 34 significantly improved its thermal stability and flexibility, since 0.5 and 1.0 % (wt. /wt.) ABM led
- 35 to 490 and 432% improvement in elongation, respectively. Furthermore, the ternary blend films in
- 36 contact with Salmonella enteritidis (S. enteritidis) showed significant inhibition to growth for 24
- 37 h, but some bacterial cells grew when the film were removed. This study demonstrates the
- 38 fabrication of ABM tuned potential biopolymer packaging flexible blend with bacteriostatic
- 39 properties.

1. Introduction

41

47

51

60

61

42 The need for biodegradable polymer packaging systems in recent times has led to increased interest 43 in research on substitutes to the recalcitrant polymer systems, especially in the current situation of 44 surging plastic usage. Polymers from renewable sources currently being explored include starch, 45 proteins and cellulose, synthetic polymers obtained from natural monomers like polylactic acid 46 (PLA) and polymers obtained from microbial fermentation (Yu, Dean, & Li., 2006). In comparison with petroleum-based polymers, the properties of renewably sourced polymers are inferior and require structural tuning for use in similar fields of application. This tuning has mostly been 48 49 advanced in thermoplastics through polymer blending. 50 PLA, a widely used high strength and modulus polymer is easily processed with other biopolymers with similar melting temperatures to design biomaterials. This helps in offsetting its extreme 52 brittleness which limits its application (Li & Micheal, 2011; Garlotta, 2001; Al-Itry, Lamnawar, 53 & Maazouz., 2014). Hence, blending PLA with elastomers and plasticizers (Tabasi, Najarzadeh, 54 & Ajji., 2015) makes possible, the design of soft biomaterials and flexible biodegradable 55 packaging systems. PBAT can suitably blend with PLA, offering good thermal stability, flexibility, 56 exceptional toughness and biodegradability (Ki & Park, 2001). Blending PBAT with soy meal 57 (Zhou, Mohanty, & Misra., 2013), starch (Brandelero, Yamashita, & Grossmann., 2010) and corn gluten meal (Reddy, Misra & Mohanty., 2014) has been reported as approach that could balance 58 59 the cost and properties of PBAT for consideration in a wider field of applications. ABM also has good thermal stability and conversion into plastic structure. Re-orientation of its proteins at about 135 °C led to the formation a bioplastic material (Sharma, Hodges, & Luzinov., 62 2008). Besides, a clinical study of antimicrobial activity of ABM showed that it inhibits microbial 63 growth, due to the presence of the lysozyme which lethally interacts with bacteria (Baron &

64 Rehault, 2007; Jones, Mandal, & Sharma., 2015). These attractive properties make ABM a 65 promising biomaterial for polymer structural tuning to enhance performance, bioactivity, 66 biodegradability, barrier properties and antimicrobial activity. 67 Most PLA binary blends show inferior mechanical properties, due to immiscibility. Attempted 68 blends such as PLA/poly (ether-b-amide) (PEBA) (Zhang, Nagarajan, Misra, & Mohanty, 2014), 69 PLA/PBAT (Arruda, Magaton, Bretas, & Ueki., 2015), PLA/PCL (Tabasi, Najarzadeh, & Ajji., 70 2015) and PLA/PHB blends (Jandas, Mohanty, & Nayak., 2014) mostly revealed poor mechanical 71 properties, due to differences in chemical structural of the constituent polymers in each case. 72 Hence, compatibilization or modification of the microstructure is a necessity in most PLA 73 biopolymer blends (Ojijo, Ray, & Sadiku, 2013; Li & Shimizu, 2009; Dong et al., 2015). Also, 74 blending with a third polymer possible means of obtaining desirable properties not attainable in 75 binary blends. Ternary blends of PLA, poly (3-hydroxybutyrateco-hydroxyvalerate) (PHBV), and poly (butylene succinate) (PBS) (PLA/PHBV PBS) revealed excellent toughness and thermal 76 77 stability due to developed favorable morphology and synergistic effects of each polymer (Zhang, 78 Mohanty, & Misra., 2012). Additionally, a blend of PLAs with poly (L-latide) (PLLA), poly (D-79 lactide) (PDLA), and poly (methyl methacrylate) (PMMA) revealed that 30-40% of PMMA 80 enhanced crystal nucleation and miscible morphologies, subsequently leading to superior storage 81 modulus and resistance to thermal deformation in the ternary blends, as compared to the binary 82 PLLA/PMMA blends (Samuel et al., 2013). These emphasize the essence of structural tuning in 83 binary blends. The study reported here probes the effect of ABM on the microstructure, 84 mechanical and antimicrobial properties of PBAT/PLA 70/30 immiscible blends. We hypothesized that the weakness of the interface of PBAT/PLA binary blend could be minimized 85

- by blending with small amount of ABM to produce biodegradable, bioactive and potential
- 87 antimicrobial PBAT/PLA/ABM ternary system with synergistic properties.

2. Materials and methods

89 *2.1 Chemicals*

- 90 PBAT (Ecoflex F blend C 1200 was obtained as a research sample from BASF Corporation, Villa
- 91 Park, IL, USA. PLA (IngeoTM biopolymer 3051D) was purchased from NatureWorks LLC,
- 92 Minnetonka, MN, USA. Egg white [albumen (ABM)] was purchased from Barry Farms,
- Wapakoneta, OH, and used as received. Chloroform (CHCl₃, \geq 99 %), used to dissolve the pelleted
- 94 polymers, was of HPLC grade, and methanol (CH₃OH, ≥99.9 %), used to precipitate the blend
- 95 from the solvent were bought from Sigma Aldrich, St. Louis, MO. Brilliant Green Sulfa Agar (BG-
- 96 Sulfa) and Tryptic Soy Broth (TSB) were purchased from Thermo Fisher Scientific, Lenexa, KS,
- 97 USA and Acumedia-Neogen Cooperation, MI, USA respectively. The bacterium, Salmonella
- 98 *enteritidis* (*S. enteritidis*) (ATCC 13076) was purchased from American Type Culture Collection
- 99 (ATCC), Manassas, VA, USA.
- 100 2.2 Incorporation of ABM in the blends
- 101 In order to homogeneously incorporate the ABM with the polymer blend, 150 g of 70/30
- 102 PBAT/PLA was blended in 500 mL of CHCl₃ for at least 12 h at 400 rpm on magnetic stirrer
- 103 (CIMAREC, Barnstead International). ABM was then added to make 2, 1.5, 1.0 and 0.5 wt. /wt.
- 104 % of the blends by first dispersing in 60 mL CHCl₃ on a magnetic stirrer (Sigma Aldrich, IKA
- 105 WORKS, Inc.) at 600 rpm for 30 min before adding to each melt blend of PBAT/PLA 70/30 and
- then mixing for 4 hrs. After this, the mixture was further homogenized by mechanical stirring for
- 5 min, before excess (800 mL) CH₃OH was added in steps of 100 mL while mechanically stirring

to precipitate the mixture. The precipitate was vacuum filtered (100 mm WhatmanTM filters) for 20 min and the powder dried at 40 °C for at least 6 h in an oven (Isotemp 200 Series).

2.3 Extrusion of polymer blend films

108

109

110

111

112

113

114

115

116

117

118

119

120

121

122

123

124

125

126

128

129

About 150 g of each of the precipitated blends containing ABM was dried for 12 h at 60 °C in a hopper (DRI-AIR Industries Inc., model RH5). This was then fed into a table top single screw extruder (Wayne SN: 8001) driven by 2 hp motor. Thermostat controlled heating zones (five) and rotation of the screw facilitated mixing and formation of continuous viscous melts for the extrusion of plastic sheets. Three heating zone are located on the barrel while two are in the die zone. The optimum working temperatures were 160, 160, 160, 157 and 156 °C, for the barrel and die zones respectively. The high barrel temperature causes the polymer to melt and randomly orient the particulates within the flowing matrix while the screw rotation induces high velocity in the matrix, causing large shear forces which contribute to the random distribution of the particles. Typically, 35 mm (w) \times 0.2 mm (t) blend specimens were collected at the die orifice at a screw speed of 20 rpm and feed rate of 4.4 g/min. The collected sheets were drawn through water stationed at the orifice of the die for quenching. The PD-mini extrusion die (SN # 13-33386) which is 6-inch deep, 3-inch tall, 6.5-inch wide with 4-inch lip opening was purchased from Premier Die Corp. Chippewa Falls, WI. These sheets were then stored in a high vacuum desiccator (JEOL, EMDSC-U10A) for later characterization. At least six specimens were used for each characterization.

127 2.4.1 Raman analysis

Molecular vibrational spectroscopy analysis of the pristine and blended polymer systems were achieved through the use of DXR Raman microscopy (Thermo Scientific). This test was performed

2.4 Determination material properties and characterization

- using a 532 nm laser (5.0 mW power), filter and grating. OMNIC Software was used for data
- acquisition and analysis.
- 132 2.4.2 X-Ray diffraction (XRD) analysis
- 133 The XRD analysis of the specimens was performed using a Rigaku diffractometer (DMAX 2100)
- equipped with Cu Kα radiation. The equipment was operated at step size of 0.02°, scan rate of
- 135 1°/min, Bragg's angle of $2\theta = 3^{\circ}$ to 80° , tube voltage and current of 40 kV and 30 mA respectively.
- 136 *2.4.5 X-Ray photoelectron spectroscopy (XPS)*
- 137 The surface composition of the blends containing ABM was analyzed using XPS. The XPS spectra
- were acquired using K-alpha surface analysis system (Thermo Scientific) equipped with Al
- monochromator as radiation source operated at 12 keV and 12 mA.
- 140 *2.4.6 Transmission electron microscopy (TEM)*
- 141 A JEOL 2010 TEM was used to analyze ABM. One (1) mg of the ABM specimen was dispersed
- in 5 mL CH₃CH₂OH for 10 min in an ultrasonic bath and a drop of the colloidal solution was
- deposited on a copper grid and analyzed.
- 144 *2.4.7 Differential scanning calorimetry (DSC)*
- 145 A TA Q 2000 DSC was used to study the thermal transitions of the specimens. Samples of 10.0 \pm
- 146 0.1 mg were used in the test. Each specimen was cooled at 20.0 °C/min from room temperature to
- -40 °C and subsequently heated from -40 °C to 200 °C at 5 °C/min and held at constant temperature
- 148 for 2.0 min. It was again cooled from 200 °C to -40 °C at 20.0 °C/min before finally scanning at
- 149 5.0 °C/min from -40 °C to 200 °C.
- 150 2.4.8 Thermogravimetric analysis (TGA)
- Thermogravimetric analysis was carried out with TA Q 500 equipment. Samples of 14 ± 0.2 mg
- were place in platinum pans. An empty platinum pan was used as a reference. Each sample was

- heated from 30 °C to 600 °C in a 50 mL/min flow of N₂. A heating rate of 5 °C/min was used to
- 154 collect data of the changes in mass as the sample was heated until it turns to char.
- 155 *2.4.9 Tensile testing*
- Measurement of tensile mechanical properties was performed using Zwick Roell Z2.5 mechanical
- testing system equipped with TestXpert data acquisition and analysis software, accordance to
- 158 ASTM D 882. Crosshead speed of 500 mm/min, 2.0 kN load cell, wedge grips and 20 mm gauge
- length were used to collect the mechanical performance data of each specimen. Specimens were
- 160 cut from the extruded polymer blend sheets to 19 mm x 0.2 mm x 120 mm and tested. At least 12
- specimens of each category were tested, averaged and reported.
- 162 *2.4.10 Light transmission and film transparency*
- The light transmission and transparency of the films was measured in the visible range (380-800)
- nm) using a visible spectrophotometer (Vernier SpectroVis Plus, Beaverton, OR) according to the
- 165 method of **Shiku et al. (2004).**
- 166 2.4. 11 Scanning electron microscopy (SEM)
- Microstructure and blend morphologies were probed using a JEOL JSM-5800 SEM. Samples were
- placed on a carbon tape fastened onto the sample holder of the SEM and sputter coated with Au-
- Pd for 5 min in a Hummer 6.2 sputtering system. The sputtering was done in a N₂ atmosphere at
- 170 20 millitorr, 5 V and 15 mA. Fractured surfaces of the tensile specimens were examined using
- 171 Hitachi S-3400N SEM.
- 172 *2.5* Antimicrobial studies of the blend systems
- 173 2.5.1 Film preparation for antimicrobial study

The extruded films were cut to 1.5 × 1.5 cm² (2.25 cm² area) with sterile scissors and exposed to

UV light for 30 min in a PCR Workstation (Air Clean® 600, Serial # 42991). These film pieces

were then stored in sterile petri dishes for later use in antimicrobial testing.

2.5.2 Antimicrobial testing

Brilliant green sulfa (BG-Sulfa) agar and tryptic soy broth (TSB) were used in the antimicrobial study of the films. In order to assess the antimicrobial activity, bacterial isolate was streaked onto BG-Sulfa agar plates and incubated at 37 °C to obtain single colonies. Using sterile disposable inoculating loops, about 3 to 5 isolated colonies were transferred from each plate into sterile tubes containing 1.5 ml of TSB. The bacterial culture was vortexed and incubated at 37 °C on a shaker at 350 rpm for about 2 h. Sterile TSB was used to adjust the turbidity of the *S. enteritidis* suspensions to obtain approximately equal optical density (OD) to that of 0.5 McFarland Standard. The OD of each bacterial suspension was measured at 600 nm (OD₆₀₀) using UV-VIS spectrophotometer (Nanodrop 2000c, Wilmington, DE, USA). The starting bacterial concentrations measured at OD₆₀₀ ranged from 0.098 to 0.112.

Antimicrobial properties of the films were tested qualitatively by directly immersing the films in 5.9×10^6 CFU/mL concentration of bacterial suspension for 4 h and then removing the films to allow all liquid TSB to dry for 10 minutes under the biosafety hood. The dried films were placed on BG-Sulfa agar plates to assess the ability of the bacteria to adhere on the film surfaces and whether their growth will be inhibited. *S. enteritidis* was chosen based on common prevalence of these organisms as foodborne pathogens, their ability to survive and multiply in most food storage temperatures (+ 4 °C) and as representative pathogens of gram negative bacteria. In this experiment, tests were done in triplicates using *S. enteritidis* bacteria. The treated dry films were placed on agar plates and incubated at 37 °C. After 24 h, films were removed with sterile forceps

and discarded, while the plates were re-incubated for additional 24 h. All plates were visually inspected after 24 h of incubation for any growth. Images of the plates were collected using an Alpha Innotech Multiimager II instrument (SN#: 510133; model: AlphaImager HP, Alpha Innotech Corp. San Leandro CA, USA). Control plates were inoculated with sterile TSB and growth control plates were inoculated with 20 μ L of the bacteria. The PBAT/PLA binary film was used as a control to check the effect of ABM on the antimicrobial properties.

203 2.6 Statistical analysis

197

198

199

200

201

202

207

- The statistical significance of differences in thermal properties was determined with a one-way analysis of variance (ANOVA) and Tukey's multiple-comparison tests. In all cases, a value of p<0.05 was considered to be significant. GraphPad Prism 7.03 software was used to do this
- 208 3. Results and discussion

analysis.

- 209 3.1 XPS and TEM analysis of ABM
- 210 Figure 1 shows (a) an XPS spectrum (b) and TEM micrograph of ABM. The composition and 211 chemical states of the ABM are shown by the XPS spectrum in **Figure 1a**. The material consists 212 of S, Cl, C, N, O and Na. The peaks at 164, 198, 285, 400, 532, 976.2-978.0 and 1071 eV are due 213 to S2p, Cl2p, C1s, N1s, O1s, O_{KLL} and Na1s transitions respectively (Demri & Muster, 1995; 214 Rouxhet et al., 2008; Aeimbhu, James, & Singjail., 2005). The atomic percentages of each element 215 suggest that C (64.35 %), O (18.74 %) and N (14.93 %) are the main constituents of ABM, while 216 the minerals (S, Cl and Na) detected in the surface analysis constitute the remaining 1.98 %. The 217 C, N and O could be due to organic molecules such as proteins and carbohydrates in the albumen. 218 Reports show that ABM has a complex protein content (ovalbumens, ovotransferrin, ovomucoid, 219 globulins, and lysozyme), low fat, minerals (chloride, sodium, Sulphur, potassium, calcium, 220 magnesium and iron) and carbohydrates (glucose, galactose, mannose, glucosamine,

galactosamine and sialic acids) (Baron et al., 2016; Brand, Dachmann, Pichler, Lotz, & Kulozik., 2016; Mine, 1995). This supports our XPS result for ABM. The micrograph in **Figure 1b** reveals a network bridge-like structure of ABM. The structure is typically amorphous. This submicron (0.5 µm wide) giant and complex assembly of molecules has an elongated morphology which suggests that in the right environment, it can possibly interconnect or bridge different molecules at the interface. This has the potential to be used as an interfacial modifier needed to offset the weakness in immiscible polymer blends.

228 3.2 Raman microanalysis

221

222

223

224

225

226

227

229

230

231

232

233

234

235

236

237

238

239

240

241

242

243

Raman spectroscopy helps in structural elucidation of molecules at the functional group level through laser induced molecular excitations (Furukawa et al., 2006). This test helped in the identification and assignment of the functional groups in the structure of the blend and due to its individual components. **Figure 2** shows the micro-Raman spectra of polymer systems in the region of 2500 to 500 cm⁻¹ using 532 nm laser excitation. It is evident that the vibrational bands for the binary (b) and ternary (a) blends in **Figure 2** are similar. The Raman spectra revealed distinct vibrational frequencies due to PBAT in the blend that appeared at 637, 1720, 1618, 1185 cm⁻¹. These are due to aromatic ring vibrations, -C=O stretching, aromatic -C=C, and -C-O-C stretching in the structure of the soft PBAT polymer respectively. These spectral assignments are in agreement with previous reports in this system (Nobrega, Olivato, Muller, & Yamashita., 2012; Furukawa et al., 2006; Kister, Cassanas, & Vert., 1998). The presence of the ABM in the ternary blend is revealed through the bands at 1010 and 1670 cm⁻¹, due to phenyl alanine aromatic breathing and amide I vibrations (Vandenabeele et al., 2000). The bands at 709 and 860 cm⁻¹ are due to -C=O out-of-plane deformation and -C-COO stretching for PLA respectively. Bands at 1050 and 1109 cm⁻¹ are ascribed to -C-CH₃ and -COC- stretching while 1395 and 2950 cm⁻¹ are

due to -CH₃ symmetric deformation, 1461 and 3004 cm⁻¹ are attributed to -CH₃ asymmetric deformation, and 1290 cm⁻¹ is as a result of -CH bending in PLA (Furukawa et al., 2007; Kister, Cassanas, & Vert., 1998). The spectrum for the ABM (Figure 2c) reveals the existence of amide I (-C=O, 1670 cm⁻¹), amide III (N-H, C-N-H, 1100-1280 cm⁻¹), -CH₂ scissoring (1482 cm⁻¹), and aromatic breathing (1010 cm⁻¹) bands, as reported elsewhere (Vandenabeele et al., 2000). The identification of bands attributed to each individual polymer suggests that the interaction between the components of the blend is largely physical in nature. 3.3 *XRD* analysis of polymer blend systems The morphology of the blends and the pure systems analyzed by X-ray diffraction is shown in Figure S1. Diffraction patterns are for; PBAT/PLA 70/30 (Figure S1 a), PBAT/PLA 70/30 composites (**Figure S1 b-e**), and ABM (**Figure S1 f**). A semicrystalline diffraction pattern within which an amorphous curve lies below four major crystalline peaks at diffraction angles of 2θ = 17.5°, 20.0°, 23.1° and 24.3° was observed in the 70/30 blend and in the ternary system. These crystalline peaks are due to PBAT. The amorphous peak of PLA merges with the amorphous region of PBAT in the blend. Similar diffraction pattern has been reported for PBAT/PLA blends with different ratios (Arruda, Magaton, Brestas, & Ueki., 2015). ABM also revealed a semicrystalline pattern, shown in **Figure S1** f. The semicrystalline microstructure of the ternary blend is critical to morphology-related structural properties, especially, stiffness and flexibility. The presence of ABM in the ternary blend is attributed to the maximum intensity in the range of $2\theta = 9-12^{\circ}$. Crystallinity has been found to alter mechanical properties in polymer blends (Li et al., 2015; Samuel et al., 2013). Hence, the addition of semicrystalline ABM into the binary 70/30 blend may potentially alter the blend morphology and microstructure to enhance the interfacial weakness and hydrophilicity of the immiscible blend as well as potentially imparting antimicrobial activity into

244

245

246

247

248

249

250

251

252

253

254

255

256

257

258

259

260

261

262

263

264

265

the biofilm. Past studies have demonstrated the influence of nanomaterials on the tuning of polymer structures and their resulting mechanical and thermal properties (Mofokeng & Luyt, 269 2015). ABM can potentially serve a similar purpose in the PBAT/PLA blend.

270 *3.4 Differential scanning calorimetry*

271

272

273

274

275

276

277

278

279

280

281

282

283

284

285

286

287

288

289

DSC heating curves of ABM, PBAT/PLA 70/30 and PBAT/PLA/ABM ternary blends incorporated with 0.5 to 2 wt. % of ABM after crystallization from melts obtained at 5 °C/min is shown in **Figure S2**. The PLA in the blend displayed a glass transition temperature at 60.20 °C, cold crystallization at 104.83 °C, and a double melting point at 148.75 °C and 156.48 °C. The PBAT melted at 122.74 with a thermal signature that merges with that of ABM, which shows a broad endothermic peak at ~ 137 °C. The denaturation point of ABM is consistent with the finding elsewhere for ABM proteins (Sharma, Hudges, & Luzinov., 2008) Comparing the curves in Figure **S2**, it is evident that the cold crystallization temperature of PLA is shifted by to lower temperature by 3-4 °C in the ternary blends, indicating enhanced cold crystallizability of the PLA due to the ABM, as observed in other studies (Labarbe Grau, Gadenne, Alfos, & Cramail., 2015). The occurrence of two distinct melting temperatures in all the blends, attributed to the individual polymers, indicates immiscibility in the blends as revealed in the microstructural analysis and past observations (Arruda, Magaton, Bretas, & Ueki., 2015). The double melting peaks of the PLA is attributed to less perfect crystals which melt at lower temperatures and more structurally perfect crystals melt at higher temperature (Jiang, Walcott, & Zhang., 2006). A second possible origin of the double melting peaks could be wide molecular weight distribution in the PLA. Lower molecular weight moieties of PLA will melt at low temperature compared to higher molecular weight moieties in the same polymer. This double melting peak is dramatically reduced in the ternary blend, indicating that albumen enhances the crystallization of the imperfect crystals of PLA

in the blend during the cold crystallization process, leading to a single melting temperature at 157

291 °C.

292

293

294

295

296

297

298

299

300

301

302

303

304

305

306

307

308

309

310

311

312

3.5 Thermogravimetric analysis (TGA)

The results on the thermal stability of the polymer blend systems by TGA are shown in **Figure S3** and **Table 1**. As evident in **Figure S3**, the inclusion of ABM to the 70/30 blend led to significant improvement in the thermal stability. Generally, the curves of the blends (Figure S3) show twostep degradation, due to less stable PLA (first) and more stable PBAT (second). The following improvements due to ABM were observed; onset of degradation, 7-25 °C, T_{d50}, 9-11 °C, T_{dmax2}, 5-7 °C, and residual yield of about 3-4 % from the binary blend. The study of PVDF/PMMA blend revealed improved T_{donset} and T_{50%} by 10.5 and 30 °C respectively, due to the addition of 6 % nanocellulose crystals (Zhang et al., 2015). Also, in PLA/PHB blend incorporated with nanoclays, the thermal stability improved significantly, due to decrease in oxygen permeability as a result of to the "crooked path" effect in the altered microstructure which delays the infiltration of oxygen and volatile degradation products which usually accelerate combustion (Jandas, Mohanty, & Nayak., 2013). These previous observations are in agreement with our findings for blends incorporating a small amount of ABM in the 70/30 blend, as depicted in the residual yields in Table 1. The degradation temperature of the PLA (T_{dmax1}) in the ternary blend was observed to decrease in the ternary blend. This is probably due to the amorphous nature of the PLA domains serving as an avenue for permeation of volatile combustions products, and since there is no order in the PLA

structure the inclusion of ABM might have increased the entropy in its domains to promote

3.6 Tensile Analysis

combustion.

The tensile analysis of the PBAT/PLA and PBAT/PLA/ABM blend systems is shown in **Figure 3. Figure 3** presents the stress-strain curve representing the general mechanical behavior of the polymeric systems under tensile force (2.0 kN). **Table 2** summarizes the tensile strength, elastic modulus, and strain at maximum load respectively. The binary PBAT/PLA 70/30 blend showed moderate ductility. **Figure 3** reveals that the binary blend fails at 526% strain. The addition of 0.5 and 1.0% of ABM into the matrix of the binary blend produced a ternary blend with a large increase in elongation with a strain at maximum loads of 1016% and 958%, respectively. These are improvements of 490% and 432% in comparison to the binary blend for 0.5 and 1.0 % additions of ABM in the ternary blend, respectively. The addition of 1.5% and 2% ABM reduced the ductility of the blend to 372% and 506% strain, respectively, and also reduced the elastic modulus. The ductility and modulus of the high-ABM-concentration blend are lower than the binary blend, suggesting that the addition of higher concentrations of the ABM led to compromise in the structural properties due to the detrimental agglomeration effects of ABM in the matrix of the blend. Also, the blends showed distinct yielding, followed by considerable cold drawing during the tensile test, indicating significant transformation of the microstructure to favor ductile fracture due to blending with the ABM. The yield strength in ternary blends with 0.5%, 1.0% and 1.5% of ABM rather lower than that of the binary blend. With 2.0% of ABM, however, similar yield strength was realized for both binary and ternary blends. The tensile strength and modulus (Table 2) were slightly less in the ternary blends, compared to the binary blend. The ternary blends revealed essentially the same strength and modulus, regardless of the amount of ABM. This is because ABM has much weaker strength and stiffness but is better in toughness than PLA. The strain at maximum load in **Table 2** revealed that specimens with 0.5% and 1.0%

313

314

315

316

317

318

319

320

321

322

323

324

325

326

327

328

329

330

331

332

333

334

ABM could endure more load while being stretched compared to the binary and ternary blends with higher content of ABM. Similar trends in property modification have been reported with the use of nanomaterials in immiscible blends (Mofokeng, & Luyt, 2015), reactive and non-reactive compatibilized polymer blends (Ojijo, Ray, & Sadiku, 2013; Li & Shimizu, 2009; Dong et al., 2015) and in composites (Rahman, Netravali, Tiimob, & Rangari, 2014; Tiimob, Rangari, & Jeelani, 2014; Tiimob, Rangari, & Jeelani, 2016). Hence, ABM tuned the microstructure of the binary blend to improve the strain to failure of the biodegradable ternary blend. 3.7 SEM analysis The morphology of the PBAT/PLA 70/30 binary blend revealed a heterogeneous phase, with ellipsoids domains of PLA dispersed in a continuous phase of PBAT (Figure S4 a). The domain sizes of about 10-40 µm. The observation of coarse domains in the phase separated "sea-island" structure indicates that the PBAT and PLA are immiscible. This is similar to findings in previous reports on PPC/PMMA (Li & Shimazu., 2009), PLLA/ABS (Dong et al., 2015), PCL/PLA (Chen et al., 2014), PLA/PBSA (Ojijo, Ray, & Sadiku, 2013), and PLA/PHBV/PBS (Zhang, Mohanty & Misra., 2012) where phase segregated morphologies have been reported. The toughening effect of ABM on the ternary blend investigated through SEM analysis of the fractured surfaces after tensile tests are shown in the micrograph in Figure S4 c. The fractured surface of the pure 70/30 blend (**Figure S4 b**) reveals a microstructure which suggests a pull out of one phase from another. The deep crack created as a result of the pull out of the phase-segregated PLA in PBAT matrix affirms the immiscibility and poor interfacial interaction existing in the binary blend. However, the fractured surface of the PBAT/PLA/ABM ternary blend (**Figure S4 c**) reveals several necked regions, suggesting some resistance to the tensile force. This surface

(Figure S4 c) show rough and tortuous morphologies with discontinuous crack paths diverted

336

337

338

339

340

341

342

343

344

345

346

347

348

349

350

351

352

353

354

355

356

357

around irregular fibrils of the matrix. This explains the enormous improvement in the toughness of the PBAT/PLA blends with 0.5% and 1.0% ABM. Interfacial interaction between dispersed domains and the matrix plays a crucial role in the toughening of a blend. High toughening effect is achieved when the dispersed phase strongly interactions with the matrix, inhibiting crack growth (Zhang, Nagarjan, Misra, & Mohanty., 2014). Hence, phase segregation in immiscibility helps in the toughening of materials through crack path interruption which delays failure, as observed in toughened blends of PLA/PEBA (Zhang, Nagarjan, Misra, & Mohanty., 2014), PLA/PCL (Tabasi, Najarzadeh, & Ajji., 2015), PLA/PBAT (Arruda, Magaton, Brestas, & Ueki., 2015) and PLA/PHB (Jandas, Mohanty, & Nayak., 2014) which revealed similar morphologies to that of PBAT/PLA/ABM. 3.8. Light transmission analysis on films The transmission of visible light at wavelength range between 380-800 nm of PBAT/PLA neat film and a PBAT/PLA/ABM ternary films with different percentages of ABM are presented in Table 3. The neat blend (PBAT/PLA) generally showed high light transmittance, and a value of 60.17 % transmission at 600 nm but the ternary films generally revealed much less (less than half of that transmitted through the neat blend) transmission of visible light due to the inclusion of ABM. Though, no trend was observed as the amount of ABM increased in the ternary blend films, it is evident that the significant reduction in light transmission between neat blend and the ternary system is due to the included ABM in the films being able to absorb or scatter significant amount of visible light. This suggest that ABM is very effective at impeding light transmission through the film. Elsewhere (Ahmad, Arfat, Al-Attar, Auras & Ejaz), a reducing trend in transmittance was observed due to the inclusion of ZnO nanoparticles as UV blocking and light impeding agent in a linear low-density polyethylene films, but this ZnO was added in large amount than in our present study.

359

360

361

362

363

364

365

366

367

368

369

370

371

372

373

374

375

376

377

378

379

380

381

3.9 Antimicrobial Studies

383

384

385

386

387

388

389

390

391

392

393

394

395

396

397

398

399

400

401

402

403

404

405

The effects on the adhesion and growth of *S. enteritidis* bacteria on 1.5×1.5 cm² PBAT/PLA and PBAT/PLA/ABM films are shown in **Figure 4**. In the control specimen (**Figure 4a**), 20 μL of TSB was dispensed in the middle of the plate. In another control, 20 µL of bacterial concentration 5.9×10^6 CFU/mL was dispensed on the agar without treatment with any film (**Figure 4b**). As expected, the bacterial control revealed growth of *S. enteritidis* colonies after 24 h while the TSB showed none (Figures 4a and 4b, respectively). The absence of growth on the TSB negative control plates indicates that the broth was not contaminated, while growth from the positive control 20 µL inoculum suggests that the bacterial cells are viable. When the films were immersed in 5.9×10^6 CFU/mL *S. enteritidis* suspension, then dried and placed on agar and incubated for 24 h (Figure 4c₁-e₁), bacterial growth was evident in the PLA/PBAT binary blend as shown in **Figure 4c**₂ immediately after film removal. However, no growth was observed on those of PBAT/PLA/ABM as shown in **Figure 4 d**₂ and **4 e**₂ immediately after films were removed. After removal of the films and re-incubating the plates for additional 24 h, bacterial growth was now evident on all the plates, including those treated with PBAT/PLA/ABM (**Figures 4c₃, 4d₃** and **4e₃**). They bacterial cells were too many were too many to count in the region where PLA/PBAT binary blend (neat film) was placed were as countable number of colonies were observed in the films containing ABM. This suggests that bacteria had adhered to all the films during the 4 h immersion in the bacteria suspension at 25 °C. While the adhesion was relatively high in the binary blend film, not much adhered to the ternary films. The survival of bacteria while the PBAT/PLA/ABM films were in contact with the agar suggests that the films most likely possess bacteriostatic properties as observed in eggshell/silver tailored PBAT/PLA blends (Tiimob et al., 2017). As evident in Figure $4d_2$ - e_2 , after the films were removed, the regions previously covered by the films revealed substantial inhibition of bacterial growth after 24 h of film contact with the agar. In agreement previous report (Tiimob et al. 2017), the 70/30 blend possessed no bactericidal effects since it is just a neat polymer blend. The blending of the 0.5% and 2.0% albumen with the 70/30 system showed some antimicrobial effects, probably due to the blockage of oxygen by particulate albumen components or the presence of some lysozyme in ABM. Reduced permeation of gaseous materials prevents moisture-dependent microbial growth in food (Beltran et al., 2014). Nanocomposites based on poly (\(\epsilon\)-caprolactone) (PCL), hydroxytyrosol (HT) (natural antioxidant) and nanoclay [cloisite 30B (C30B)], were reported to have improved the poor PCL intrinsic barrier properties, leading to significant improvement in oxygen barrier in ternary nanobiocomposites containing C30B and 10 wt. % HT (Beltran, Valente, Jimenez, & Garrigos., 2014). Lysozyme protein which is inherent in albumen is responsible for its antimicrobial activity (Baron et al., 2016; Brand, Dachmann, Pichler, Lotz, & Kulozik., 2016; Mine, 1995). The bacteriostatic effects (instead of bactericidal) observed with the ternary blends could as well be associated with the existence lysozyme in minute amounts, due to the quantity of ABM used in this study, leading to insufficient lysozyme in the films. It is also possible that lysozyme may have degraded due to high temperature and chemical treatment of the albumen during the film fabrication process.

4. Conclusion

406

407

408

409

410

411

412

413

414

415

416

417

418

419

420

421

422

423

424

425

426

427

428

Extruded biodegradable poly (butylene adipate-co-terephthalate) (PBAT)/agro-based polylactic acid (PLA) binary and ternary blend films with 0.5-2.0% ABM were studied to determine the effect of the ABM on microstructure, thermal and tensile properties of the blend. The results revealed that the two polymers are immiscible, due to the presence of distinct melting points and

phase segregated morphologies in the blend and composite structures. Also, the PLA was amorphous while PBAT is semicrystalline, resulting in a semi crystalline immiscible blend. The tensile and SEM results showed that 0.5-1.0 % of ABM led to significant enhancement in the toughness due to heterogeneous phased matrices with interrupt cracks paths, diverting crack propagation and delaying failure in the ternary systems, whereas thermal analysis showed that ABM enhanced the cold crystallization and thermal stability of the ternary blends. These revealed that the PBAT/PLA/ABM 70/30/0.5 ternary blend possessed the desirable balance strength and flexibility for flexible designs and applications. *In vitro* antimicrobial study on *S. enteritidis* showed significant inhibition of bacterial growth during 24 h on contact with films, but the bacteria grew after the films were removed and the plate re-incubated for additional 24 h, suggesting bacteriostatic effects due to the inclusion of ABM in the films.

Acknowledgements

The authors very grateful for the financial support from NSF-CREST #1137681, NSF-RISE #1459007, NSF-MRI-1531934 and AL/NSF EPSCoR # 1158862 grants. The authors gratefully acknowledge use of facilities and instrumentation supported by NSF through the University of Wisconsin Materials Research Science and Engineering Center (DMR-1121288). The authors are very grateful to Tuskegee University shared instrumentation biomedical research core research facility (NIH grant G12MD007585).

References

- Aeimbhu, A., Castle, J. E., & Singjai, P. (2005). Accounting for the size of molecules in determination of adsorption isotherms by XPS; exemplified by adsorption of chicken egg albumin on titanium. *Surface and Interface Analysis*, *37*, 1127-1136.
- 451 Ahmed, J., Arfat Y. A., Al-Attar, H., Auras, R., & Ejaz M. (2017). Rheological, structural,
 452 ultraviolet protection and oxygen barrier properties of linear low-density polyethylene

453	films reinforced with zinc oxide (ZnO) nanoparticles. Food Packaging and Shelf Life, 13
454	20-26
455	Arruda, L. C., Magaton, M., Bretas, R. E. S., & Ueki, M. M. (2015). Influence of chain extender
456	on mechanical, thermal and morphological properties of blown films of PLA/PBAT
457	blends. Polymer Testing, 43, 27-37.
458	Baron, F., Nau, F., Guérin-Dubiard, C., Bonnassie, S., Gautier, M., Andrews, S. C., & Jan, S.
459	(2016). Egg white versus Salmonella Enteritidis! A harsh medium meets a resilient
460	pathogen. Food Microbiology, 53, Part B, 82-93.
461	Baron, F. R., & Rehault, S. (2007). In R., Huopalahti, Lopez-Fandino, R., M. Anton, & R.
462	Schade (Ed.), Bioactive Egg Compounds (pp. 191). Springer-Verlag: Berlin/Heidelberg.
463	Beltrán, A., Valente, A. J. M., Jiménez, A., & Garrigós, M. C. (2014). Characterization of
464	Poly(ε-caprolactone)-Based Nanocomposites Containing Hydroxytyrosol for Active Food
465	Packaging. Journal of Agricultural and Food Chemistry, 62, 2244-2252.
466	Brand, J., Dachmann, E., Pichler, M., Lotz, S., & Kulozik, U. (2016). A novel approach for
467	lysozyme and ovotransferrin fractionation from egg white by radial flow membrane
468	adsorption chromatography: Impact of product and process variables. Separation and
469	Purification Technology, 161, 44-52.
470	Brandelero, R. P. H., Yamashita, F., & Grossmann, M. V. E. (2010). The effect of surfactant
471	Tween 80 on the hydrophilicity, water vapor permeation, and the mechanical properties
472	of cassava starch and poly(butylene adipate-co-terephthalate) (PBAT) blend films.
473	Carbohydrate Polymers, 82, 1102-1109.
474	Chen, J., Lu, L., Wu, D., Yuan, L., Zhang, M., Hua, J., & Xu, J. (2014). Green Poly(ε-
475	caprolactone) Composites Reinforced with Electrospun Polylactide/Poly(ε-caprolactone)

476	Blend Fiber Mats. ACS Sustainable Chemistry & Engineering, 2, 2102-2110.
477	Demri, B., & Muster, D. (1995). XPS study of some calcium compounds. <i>Journal of Materials</i>
478	Processing Technology, 55, 311-314.
479	Dong, W., He, M., Wang, H., Ren, F., Zhang, J., Zhao, X., & Li, Y. (2015). PLLA/ABS Blends
480	Compatibilized by Reactive Comb Polymers: Double Tg Depression and Significantly
481	Improved Toughness. ACS Sustainable Chemistry & Engineering, 3, 2542-2550.
482	Furukawa, T., Sato, H., Murakami, R., Zhang, J., Noda, I., Ochiai, S., & Ozaki, Y. (2006).
483	Raman microspectroscopy study of structure, dispersibility, and crystallinity of
484	poly(hydroxybutyrate)/poly (l-lactic acid) blends. <i>Polymer</i> , 47, 3132-3140.
485	Furukawa, T., Sato, H., Murakami, R., Zhang, J., Noda, I., Ochiai, S., & Ozaki, Y. (2007).
486	Comparison of miscibility and structure of poly(3-hydroxybutyrate-co-3-
487	hydroxyhexanoate)/poly(l-lactic acid) blends with those of poly(3-
488	hydroxybutyrate)/poly(l-lactic acid) blends studied by wide angle X-ray diffraction,
489	differential scanning calorimetry, and FTIR microspectroscopy. Polymer, 48, 1749-1755.
490	Garlotta, D. (2001). A literature review of poly (lactic acid). Journal of Polymers and the
491	Environment, 9, 63-84.
492	Annual book of ASTM standards. (2002). D 882-02: Standard Test Method for Tensile
493	Properties of Thin Plastic Sheeting. (pp. 1-10). Pennsylvania: ASTM international
494	Jandas, P. J., Mohanty, S., & Nayak, S. K. (2014). Morphology and Thermal Properties of
495	Renewable Resource-Based Polymer Blend Nanocomposites Influenced by a Reactive
496	Compatibilizer. ACS Sustainable Chemistry & Engineering, 2, 377-386.
497	Jiang, L., Wolcott, M. P., & Zhang, J. (2006). Study of Biodegradable Polylactide/Poly (butylene
498	adipate-co-terephthalate) Blends. Biomacromolecules, 7, 199-207.

499 Jones, A., Mandal, A., & Sharma, S. (2015). Protein-based bioplastics and their antibacterial 500 potential. Journal of Applied Polymer Science, 132, n/a-n/a. doi:10.1002/app.41931 501 Ki, H. C., & Park, O. O. (2001). Synthesis, characterization and biodegradability of the 502 biodegradable aliphatic-aromatic random copolyesters. *Polymer*, 42, 1849-1861. 503 Kister, G., Cassanas, G., & Vert, M. (1998). Structure and morphology of solid lactide-glycolide 504 copolymers from 13C n.m.r., infra-red and Raman spectroscopy. *Polymer*, 39, 3335-505 3340. 506 Lebarbé, T., Grau, E., Gadenne, B., Alfos, C., & Cramail, H. (2015). Synthesis of Fatty Acid-507 Based Polyesters and Their Blends with Poly(l-lactide) as a Way To Tailor PLLA 508 Toughness. ACS Sustainable Chemistry & Engineering, 3, 283-292. 509 Li, H., & A., M. (2011). Effect of chain extension on the properties of PLA/TPS blends. *Journal* 510 of Applied Polymer Science, 122, 134-141. Li, L., Huang, W., Wang, B., Wei, W., Gu, Q., & Chen, P. (2015). Properties and structure of 511 polylactide/poly (3-hydroxybutyrate-co-3-hydroxyvalerate) (PLA/PHBV) blend fibers. 512 513 Polymer, 68, 183-194. 514 Li, Y., & Shimizu, H. (2009). Compatibilization by Homopolymer: Significant Improvements in 515 the Modulus and Tensile Strength of PPC/PMMA Blends by the Addition of a Small 516 Amount of PVAc. ACS Applied Materials & Interfaces, 1, 1650-1655. 517 Mine, Y. (1995). Recent advances in the understanding of egg white protein functionality. 518 *Trends in Food Science & Technology, 6, 225-232.* 519 Mofokeng, J. P., & Luyt, A. S. (2015). Morphology and thermal degradation studies of melt-520 mixed poly (lactic acid) (PLA)/poly(ε-caprolactone) (PCL) biodegradable polymer blend 521 nanocomposites with TiO2 as filler. *Polymer Testing*, 45, 93-100.

522	Nobrega, M. M., Olivato, J. B., Müller, C. M. O., & Yamashita, F. (2012). Biodegradable starch
523	based films containing saturated fatty acids: thermal, infrared and raman spectroscopic
524	characterization. <i>Polímeros</i> , 22, 467-474.
525	Ojijo, V., Ray, S. S., & Sadiku, R. (2013). Toughening of Biodegradable Polylactide/Poly
526	(butylene succinate-co-adipate) Blends via in Situ Reactive Compatibilization. ACS
527	Applied Materials & Interfaces, 5, 4266-4276.
528	Rahman, M. M., Netravali, A. N., Tiimob, B. J., & Rangari, V. K. (2014). Bioderived "Green"
529	Composite from Soy Protein and Eggshell Nanopowder. ACS Sustainable Chemistry &
530	Engineering, 2, 2329-2337.
531	Reddy, M. M., Misra, M., & Mohanty, A. K. (2014). Biodegradable Blends from Corn Gluten
532	Meal and Poly (butylene adipate-co-terephthalate) (PBAT): Studies on the Influence of
533	Plasticization and Destructurization on Rheology, Tensile Properties and Interfacial
534	Interactions. Journal of Polymers and the Environment, 22, 167-175.
535	Rouxhet, P. G., Misselyn-Bauduin, A. M., Ahimou, F., Genet, M. J., Adriaensen, Y., Desille, T.
536	Deroanne, C. (2008). XPS analysis of food products: toward chemical functions and
537	molecular compounds. Surface and Interface Analysis, 40, 718-724.
538	Samuel, C., Cayuela, J., Barakat, I., Müller, A. J., Raquez, JM., & Dubois, P. (2013).
539	Stereocomplexation of Polylactide Enhanced by Poly(methyl methacrylate): Improved
540	Processability and Thermomechanical Properties of Stereocomplexable Polylactide-
541	Based Materials. ACS Applied Materials & Interfaces, 5, 11797-11807.
542	Sharma, S., Hodges, J. N., & Luzinov, I. (2008). Biodegradable plastics from animal protein
543	coproducts: Feathermeal. Journal of Applied Polymer Science, 110, 459-467.
544	Shiku, Y., Hamaguchi, P. Y., Soottawat, B., Visessanguan, W., & Tanaka, M. (2004). Effects of

545	surimi quality on properties of edible films base on Alaska Pollack. Food Chemistry, 86,
546	493-499.
547	Tabasi, R. Y., Najarzadeh, Z., & Ajji, A. (2015). Development of high performance sealable
548	films based on biodegradable/compostable blends. Industrial Crops and Products, 72,
549	206-213.
550	Tiimob, B. J., Jeelani, S., & Rangari, V. K. (2016). Eggshell reinforced biocomposite—An
551	advanced "green" alternative structural material. Journal of Applied Polymer Science,
552	133, n/a-n/a. doi:10.1002/app.43124
553	Tiimob, B. J., Mwinyelle, G., Abdela, W., Samuel, T., Jeelani, S., & Rangari, V. K. (2017).
554	Nanoengineered Eggshell-Silver Tailored Copolyester Polymer Blend Film with
555	Antimicrobial Properties. Journal of Agricultural and Food Chemistry, 65, 1967-1976.
556	Tiimob, B. J., Rangari, V. K., & Jeelani, S. (2014). Effect of reinforcement of sustainable $\beta\text{-}$
557	CaSiO3 nanoparticles in bio-based epoxy resin system. Journal of Applied Polymer
558	Science, 131, n/a-n/a. doi:10.1002/app.40867
559	Vandenabeele, P., Wehling, B., Moens, L., Edwards, H., De Reu, M., & Van Hooydonk, G.
560	(2000). Analysis with micro-Raman spectroscopy of natural organic binding media and
561	varnishes used in art. Analytica Chimica Acta, 407, 261-274.
562	Yu, L., Dean, K., & Li, L. (2006). Polymer blends and composites from renewable resources.
563	Progress in Polymer Science, 31, 576-602.
564	Zhang, K., Mohanty, A. K., & Misra, M. (2012). Fully Biodegradable and Biorenewable Ternary
565	Blends from Polylactide, Poly(3-hydroxybutyrate-co-hydroxyvalerate) and Poly
566	(butylene succinate) with Balanced Properties. ACS Applied Materials & Interfaces, 4,
567	3091-3101.

568	Zhang, K., Nagarajan, V., Misra, M., & Mohanty, A. K. (2014). Supertoughened Renewable
569	PLA Reactive Multiphase Blends System: Phase Morphology and Performance. ACS
570	Applied Materials & Interfaces, 6, 12436-12448.
571	Zhang, Z., Wu, Q., Song, K., Ren, S., Lei, T., & Zhang, Q. (2015). Using Cellulose Nanocrystals
572	as a Sustainable Additive to Enhance Hydrophilicity, Mechanical and Thermal Properties
573	of Poly (vinylidene fluoride)/Poly (methyl methacrylate) Blend. ACS Sustainable
574	Chemistry & Engineering, 3, 574-582.
575	Zhou, X., Mohanty, A., & Misra, M. (2013). A New Biodegradable Injection Moulded Bioplastic
576	from Modified Soy Meal and Poly (butylene adipate-co-terephthalate): Effect of
577	Plasticizer and Denaturant. Journal of Polymers and the Environment, 21, 615-622.
578	
579	
580	
581	
582	
583	
584	
585	
586	
587	
588	
589	
590	
591	
592	
593	Figure captions

594	Figure 1 . Structural analysis of albumen. (a) X-ray photoelectron spectrum, (b) transmission
595	electron micrograph.
596	Figure 2. Raman spectra of polymer systems: (a) PBAT/PLA/albumen 70/30/1 blend (b)
597	PBAT/PLA 70/30 blend and (c) albumen.
598	Figure 3. Stress-strain curves of PBAT/PLA/albumen polymer blends from tensile test.
599	Figure 4. Antimicrobial effect of PBAT/PLA/albumen polymer blend: (a) Brilliant Green Sulfo
600	Agar Control, (b) 20 μL of <i>S. enteritidis</i> placed on agar as control, (c ₁ -c ₃) PBAT/PLA 70/30 blend
601	against S. enteritidis, (d ₁ -d ₃) PBAT/PLA/albumen 70/30/0.5 blend against S. enteritidis, (e ₁ -e ₃)
602	PBAT/PLA/albumen 70/30/2.0 blend against <i>S. enteritidis</i>
603	
604	
605	
606	
607	
608	
609	
610	
611	
612	
613	
614	
615	
616	Tables

Table 1. Thermal degradation of blended PBAT/PLA with albumen (ABM) determined using onset of degradation temperature (T_{donset}), temperature at 50 % degradation (T_{d50}), maximum degradation temperature T_{dmax} , and residual yield.

Specimen	$T_{ m donset}$	$T_{ m d50}$	T_{dmax1}	$T_{ m dmax2}$	Residue (%)
PBAT-PLA 70/30	288.06±5.88ab	341.52±0.95a	307.61±1.43 ^a	355.59±0.11 ^a	1.17±0.37 ^a
PBAT-PLA-ABM 0.5	295.52±1.79abe	350.06±1.03 ^{bcde}	288.74±2.20 ^b	360.79±1.19 ^{bde}	4.39±0.35 ^{bcde}
PBAT-PLA-ABM 1.0	313.81±2.26 ^{cd}	352.54±1.41 ^{bcd}	282.94±1.34 ^c	362.80±0.47 ^{cde}	4.76±0.61 ^{bcde}
PBAT-PLA-ABM 1.5	308.42±1.85 ^{cd}	350.29±0.68 ^{bcde}	277.34±0.67 ^{de}	362.10±0.50 ^{bcde}	5.04±0.66 ^{bcde}
PBAT-PLA-ABM 2.0	299.68±2.36be	346.91±2.34 ^{bde}	275.89±1.01 ^{de}	361.60±0.81 ^{bcde}	5.33±0.35 ^{bcde}

^a Mean values with dierent letters in the same column represent significant dierences (p< 0.05) among the samples according to a one-way analysis of variance (ANOVA) and Tukey's multiple-comparison tests.

Table 2. Tensile properties of PBAT/PLA/albumen polymer blend systems.

Specimen	Tensile strength	Elastic modulus	Strain (%) at	
	(MPa)	(MPa)	maximum load	
PBAT/PLA 70-30	17.41 ± 0.46 ^{abcd}	333.43 ± 78.17 ^{abcde}	525.69 ± 53.46a	
PBAT/PLA/ABM 0.5	14.14 ± 1.87 ^{abcde}	242.82 ± 53.29 ^{abcde}	1016.24 ± 116.02bc	
PBAT/PLA/ABM 1.0	14.81 ± 1.85 ^{abcde}	259.30 ± 56.42 ^{abced}	958.56 ± 150.45bc	
PBAT/PLA/ABM 1.5	14.02 ± 1.03 ^{abcde}	298.46 ± 46.24 ^{abcde}	17.89 ± 6.95^{de}	
PBAT/PLA/ABM 2.0	13.16 ± 1.79 ^{abcde}	292.17 ± 49.72 ^{abcde}	14.29 ± 6.12 ^{de}	

^a Mean values with dierent letters in the same column represent significant dierences (p< 0.05) among the samples according to a one-way analysis of variance (ANOVA) and Tukey's multiple-comparison tests.

Table 3. Light transmittance values of PBAT/PLA/albumen polymer blend systems

636 Specimen	Transmittance (%)					
	380 nm	400 nm	500 nm	600 nm	700 nm	800 nm
637BAT/PLA-70-30	40.25 ± 3.13	18.54 ± 1.93	39.81 ± 2.48	60.17 ± 2.57	65.25 ± 2.29	69.24 ± 1.89
PBAT/PLA/ABM 0.5	11.24 ± 0.58	4.95 ± 0.18	11.86 ± 0.12	21.93 ± 0.44	24.74 ± 0.80	27.39 ± 1.21
636 AT/PLA/ABM 1.0	11.44 ± 0.92	5.03 ± 0.43	12.81 ± 0.95	23.94 ± 2.10	27.05 ± 2.86	30.10 ± 3.57
PBAT/PLA/ABM 1.5	11.44 ± 0.55	5.03 ± 0.18	12.81 ± 0.53	23.94 ± 0.88	27.05 ± 1.03	30.10 ± 0.97
639 AT/PLA/ABM 2.0	9.68 ± 0.36	4.3 ± 0.17	11.08 ± 0.36	20.16 ± 0.69	29.89 ± 0.89	33.50 ± 1.13

Figures

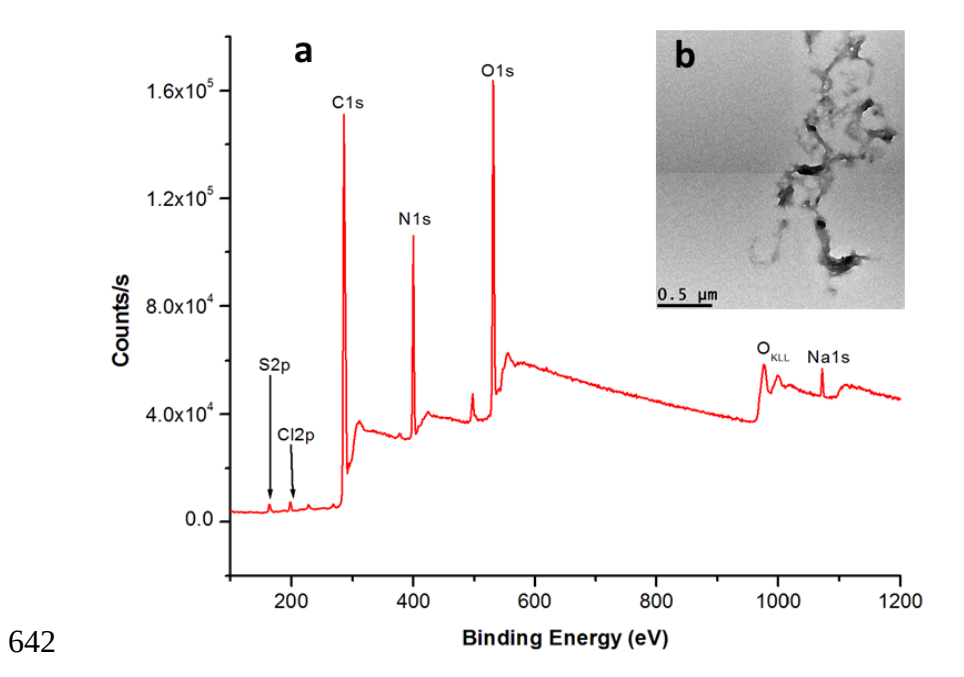


Figure 1.

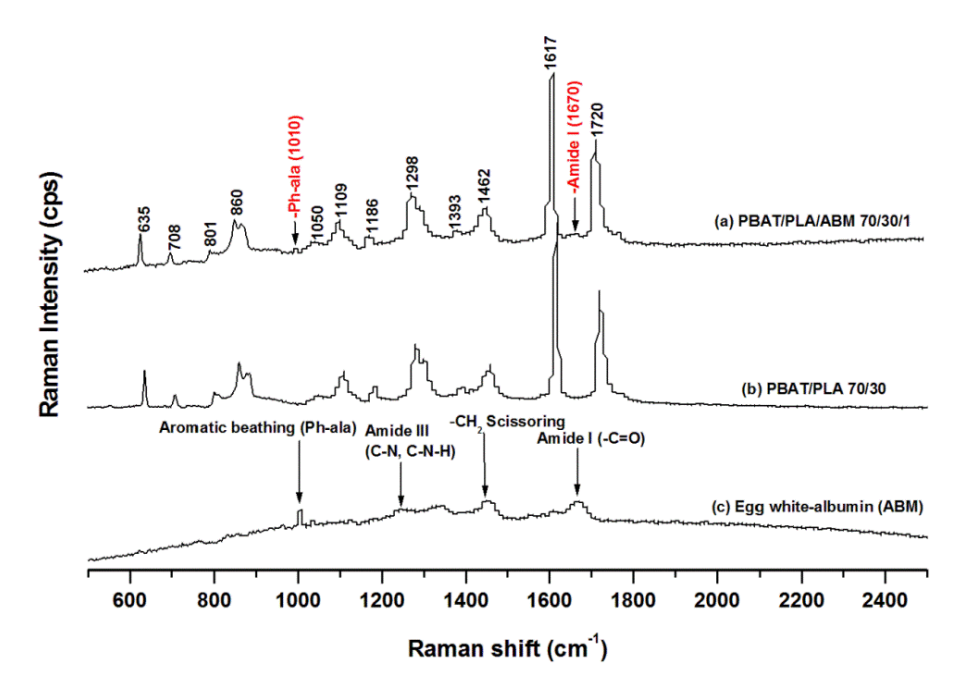


Figure 2.

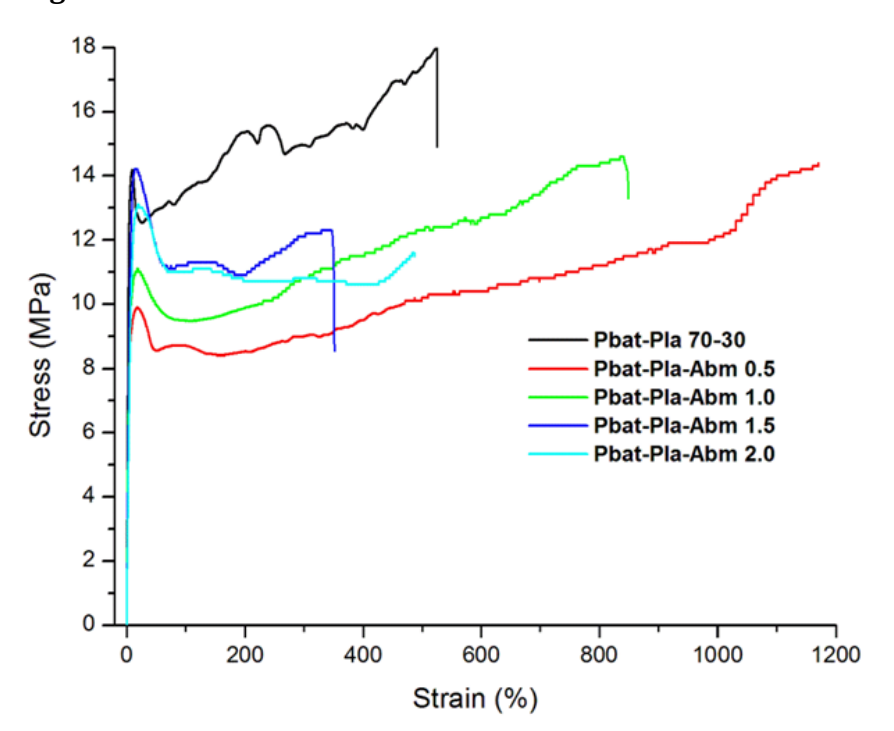


Figure 3.

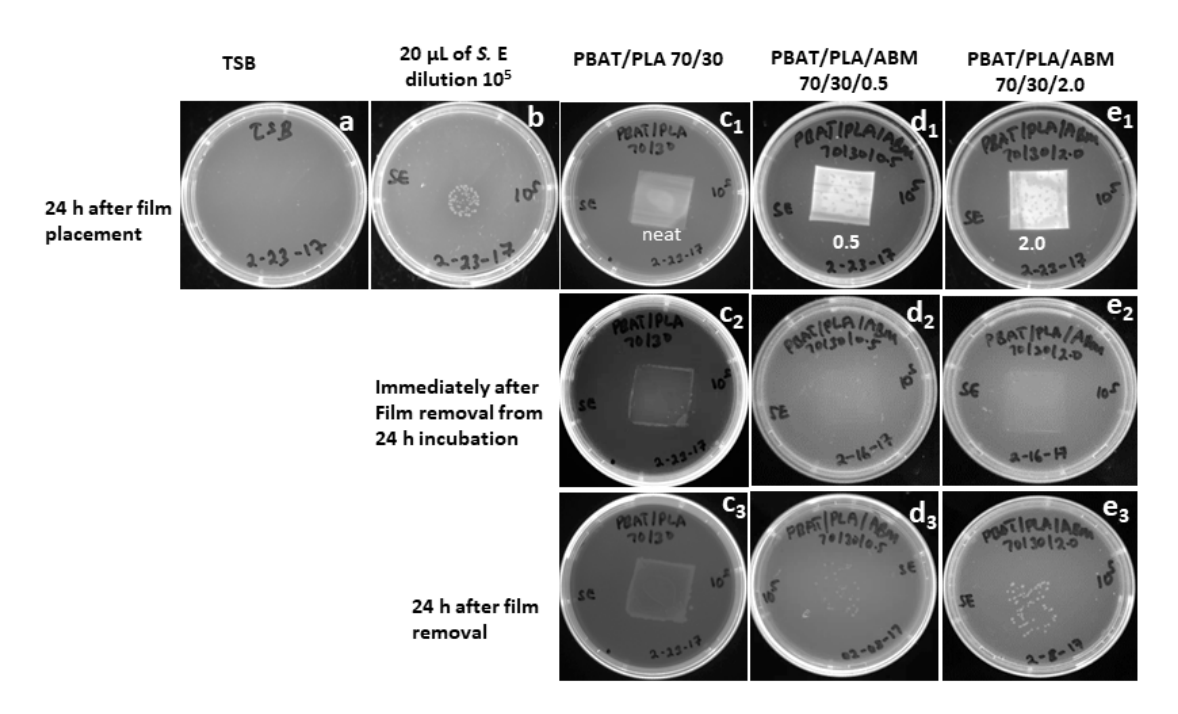


Figure 4.

- **1** Supplementary information
- 2 Tough aliphatic-aromatic copolyester and chicken egg white flexible biopolymer blend with
- 3 bacteriostatic effects
- 4 Boniface J. Tiimob^a, Vijaya K. Rangari^{a,*}, Gregory Mwinyelle^b, Woubit Abdela^b, Paul G. Evans^c,
- 5 Nicholas Abbott^c, Temesgen Samuel^b, Shaik Jeelani^a
- ^aDepartment of Materials Science and Engineering, ^bDepartment of Pathobiology, College of
- 7 Veterinary Medicine, Tuskegee University, Tuskegee, AL 36088, United States
- 8 ^cDepartment of Chemical and Biological Engineering, University of Wisconsin-Madison,
- 9 Madison, WI 53706, United States
- 10 Corresponding Author
- *(V.K.R) E-mail:rangariv@mytu.tuskegee.edu.
- 12 **Figure S1**. X-ray diffraction patterns: (a) PBAT/PLA 70/30 (b) PBAT/PLA/ABM 70/30/0.5
- 13 (c) PBAT/PLA/ABM 70/30/1 (d) PBAT/PLA/ABM 70/30/1.5 (e) PBAT/PLA/ABM 70/30/2 (f)
- 14 ABM
- 15 **Figure S2**. DSC curves for ABM and PBAT/PLA/ABM blend composites.
- **Figure S3**. Thermal degradation of PBAT/PLA/ABM polymer blends.
- 17 **Figure S4**. SEM micrographs:(a) PBAT/PLA 70/30 blend morphology; fractured surfaces after
- tensile analysis :(b) PBAT/PLA 70/30 binary blend, (c) PBAT/PLA/ABM 70/30/1ternary blend.

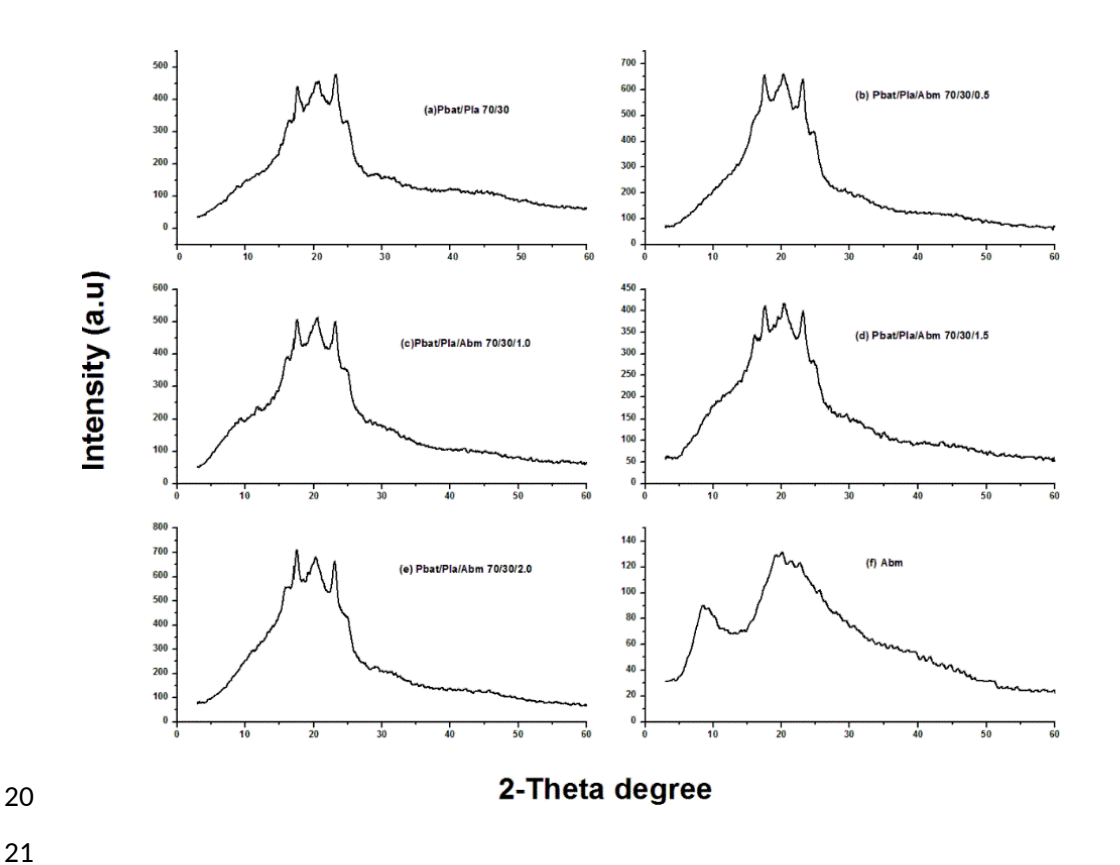


Figure S1. X-ray diffraction patterns: (a) PBAT/PLA 70/30 (b) PBAT/PLA/ABM 70/30/0.5 (c) PBAT/PLA/ABM 70/30/1 (d) PBAT/PLA/ABM 70/30/1.5 (e) PBAT/PLA/ABM 70/30/2 (f) ABM.

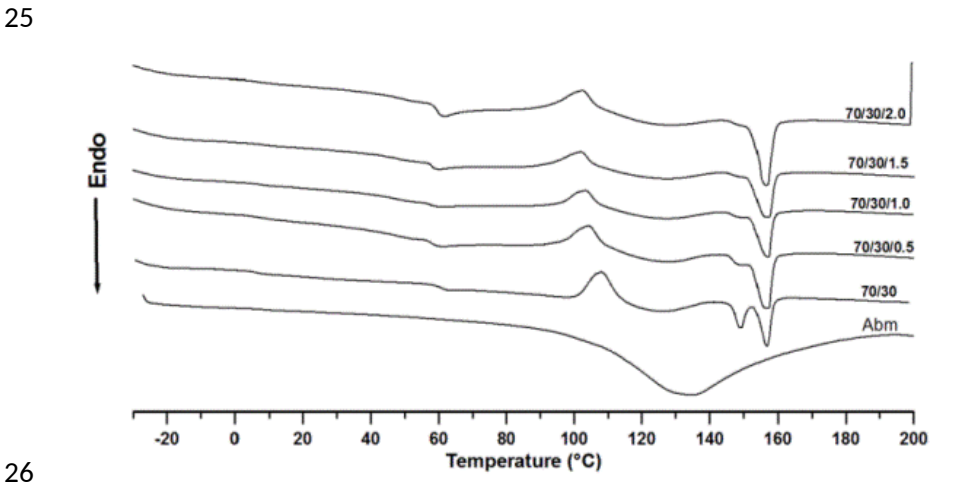


Figure S2. DSC curves for ABM and PBAT/PLA/ABM blend composites.

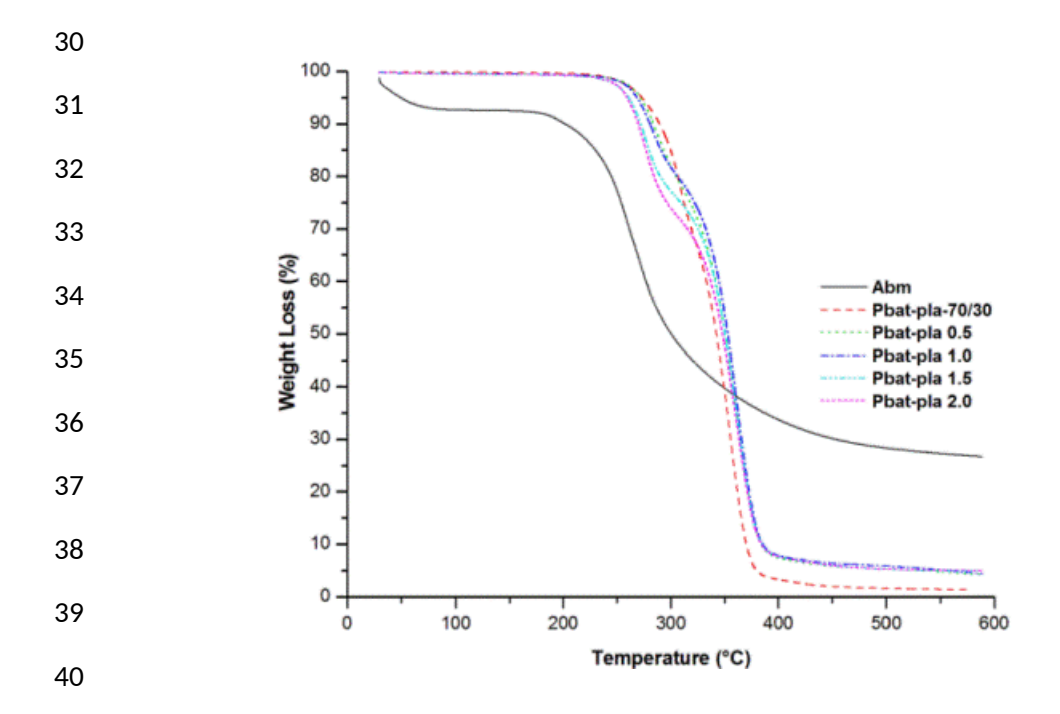


Figure S3. Thermal degradation of PBAT/PLA/ABM polymer blends.

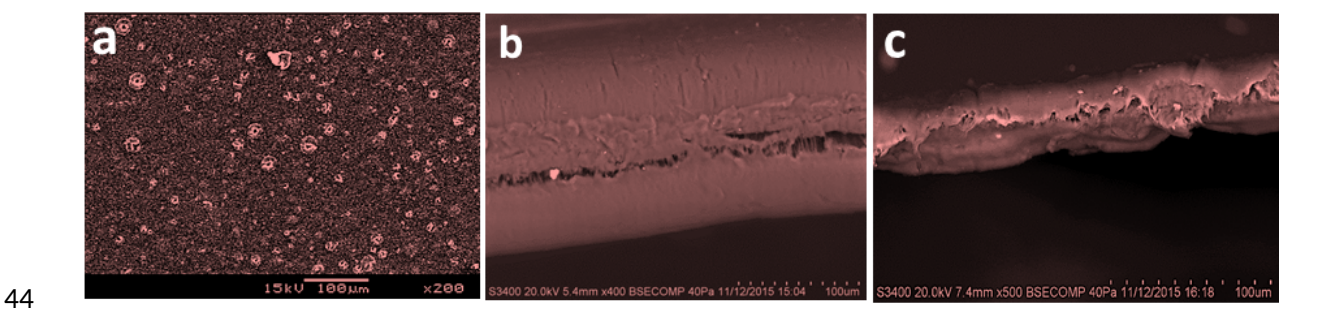


Figure S4. SEM micrographs:(a) PBAT/PLA 70/30 blend morphology; fractured surfaces after tensile analysis: (b) PBAT/PLA 70/30 binary blend, (c) PBAT/PLA/ABM 70/30/1% ABM ternary blend.